

## Experimental Validation of Color Doppler Velocity Measurement for Ultrasonic-Measurement-Integrated Simulation of Blood Flow\*

Lei LIU\*\*, Toshiyuki HAYASE\*\*\*, Makoto OHTA\*\*\*  
and Kosuke INOUE\*\*\*

\*\* Graduate School of Engineering, Tohoku University, Aramaki Aza Aoba,  
Aoba-ku, Sendai, JAPAN

E-mail: ryu@reynolds.ifs.tohoku.ac.jp

\*\*\* Institute of Fluid Science, Tohoku University, Katahira,  
Aoba-ku, Sendai, JAPAN

### Abstract

Cardiovascular diseases are closely related to blood flow. Ultrasonic-Measurement-Integrated (UMI) simulation, in which results of ultrasonic measurement are fed back to the flow simulation, was proposed in a previous study in order to reproduce the real blood flow accurately and efficiently. The usability of the UMI simulation was confirmed by numerical experiment, but the effectiveness of this simulation was strongly affected by the accuracy of the ultrasonic measurement. In this paper, we examined the accuracy of a commercial ultrasonic measurement device by an experiment with a PVA-H straight tube phantom. By analyzing the measured color Doppler images for a developed laminar flow inside the phantom, we obtained the relationship between the color Doppler value and the Doppler velocity (C-V relationship). It was revealed that the original C-V relationship provided in the device as a color bar was not suitable for quantitative evaluation of Doppler velocity to be used in UMI simulation. Compared with the original C-V relationship, the present C-V relationship results are in far better agreement with the analytic solution. Investigation of the normalized error confirmed that the result obtained with the present C-V relationship was reliable in cases of relatively high Reynolds number in the flow domain except near the wall. The two signal conditioning factors of the device had little influence on the Doppler velocity. Finally, we investigated the effect of temporal and spatial averaging of ultrasonic measurement data to clarify the relation between the number of averagings and the level of agreement with the analytic solution.

**Key words:** Ultrasonic Measurement Integrated Simulation, Blood Flow, Ultrasonic Measurement, In Vitro Validation, PVA-H

### 1. Introduction

Cardiovascular disease is one of main causes of death in many countries, the number of fatalities tending to increase with advancing age. Because of our fast-aging society, this is a problem calling for immediate attention. Previous studies have reported cardiovascular diseases to be closely related to blood flow<sup>[1-5]</sup>, and much research has been performed from

this point of view, most of which has been carried out by experimental measurement<sup>[6-10]</sup> (*in vitro* and *in vivo*) or, recently, by computational fluid dynamics (CFD).

Even with substantial improvement in measurement technology, it is still difficult to accurately measure the detailed structure of 3D blood flow, including the vessel wall shear stress and the wall pressure, important factors of cardiovascular diseases, by using existing measurement techniques, such as MRI, CT, X-ray, and ultrasonic measurement.

On the other hand, computer simulation of blood flow has also been actively conducted. A realistic solution of the blood flow can be obtained by solving the fundamental equations of the flow with realistic vessel geometry obtained by MRI or CT<sup>[9-13]</sup>. However, this method has inherent problems because it is generally difficult to accurately set boundary conditions of the blood flow and of the geometry of blood vessels, resulting in computational results that are sometimes insufficient to reproduce real blood flow.

This background indicates the necessity of finding a new way to obtain details on individual blood flow for treatment of patients suffering from cardiovascular disease and the need for fundamental research to uncover the causes of such disease. Our group has previously proposed a new method called Ultrasonic-Measurement-Integrated (UMI) simulation, in which ultrasonic measurement and CFD are integrated to reproduce blood flow<sup>[14]</sup>. UMI simulation is a kind of flow observer<sup>[15]</sup>, the components of which are shown in Fig. 1. As shown in this figure, the ultrasonic measurement result is compared with the corresponding result of the numerical simulation, and the difference of the two is fed back to the numerical simulation as a feedback signal based on the feedback law to reduce the difference. By performing successive computation to reduce the difference to zero, the actual flow is reproduced asymptotically. In previous studies, Funamoto *et al.* confirmed the usability of UMI simulation by 2-D and 3-D numerical experiments with realistic geometry of a thoracic aneurysm<sup>[16-18]</sup>. Although these numerical experiments were performed based on the assumption that there is no measurement error in ultrasonic measurement, the result of actual ultrasonic measurement inevitably contains some measurement error. Since the accuracy of the ultrasonic measurement directly influences the accuracy of UMI simulation, evaluation and improvement of the measurement accuracy are essential to develop the UMI simulation system.

There are several modes of measurement in general medical ultrasonic instrument: B-mode, M-mode, pulse Doppler mode, power Doppler mode and color Doppler mode for corresponding examination purposes<sup>[19, 20]</sup>. In the color Doppler mode, in which the information on geometry and blood flow are available at the same time, the velocity component of the fluid along the ultrasonic beam is measured based on the Doppler shift frequency, and it is converted to the intensity of colors, namely, the color Doppler value, to visualize the blood flow. Generally, the velocities toward the ultrasound probe and those away from the probe are displayed in warm and cold colors, respectively. A number of investigations have been performed on the validation of ultrasonic measurement using the fluid flow phantom<sup>[21]</sup>, the spring-type phantom<sup>[22]</sup>, and the belt-type phantom<sup>[23]</sup>.

Although the PC controlled spring-type phantom and the belt-type phantom provide steady Doppler signals, the experimental environments of these experiments are different from that

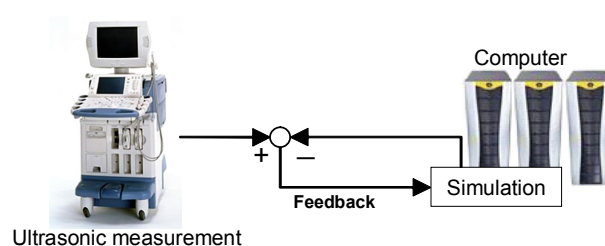


Fig. 1 Ultrasonic-measurement-integrated (UMI) simulation system

of the clinical use of ultrasonic measurement applying to the living tissue. On the other hand, the fluid flow phantom requires a complicated experimental setup, but the experimental environment is similar to that of the practical use of the ultrasonic measurement. In our previous study, we obtained the relationship between the color Doppler value and the Doppler velocity, abbreviated as “C-V relationship,” by analyzing the color bar displayed on the monitor of the ultrasonic device<sup>[14]</sup>. In order to visualize the blood flow characteristics clearly, many signal conditioning schemes such as wall filters are equipped in commercial medical ultrasonic device. The evaluation of various filters as to simple input signals and measured Doppler signal samples have been performed in previous studies<sup>[24, 25]</sup>. However, it is difficult to apply the results of the previous studies to evaluate the effect of signal processing in a commercial medical ultrasonic device to be used in UMI simulation.

In this paper, we examined the accuracy of Doppler velocity measurement using a commercial medical ultrasonic diagnostic instrument as the measurement device. We developed an *in vitro* experimental system containing a poly (vinyl alcohol) hydrogel (PVA-H) fluid flow phantom, which we then employed for ultrasonic measurement. By measuring a fully developed laminar flow in a straight circular tunnel in the phantom, we investigated the C-V relationship in the ultrasonic measurement including the effect of several signal conditioning parameters. The effects of temporal and spatial averaging of ultrasonic measurement data were also discussed.

### Nomenclature

$C$	Color Doppler value ( $0 \leq C \leq 255$ , integer value)
$D$	Diameter of the straight circular tunnel in PVA-H phantom
$E$	Normalized error in Doppler velocity $(V - V_{ana})/V_{mean}$
$E_{ave}$	Average of $E$ , $\frac{1}{y'_2 - y'_1} \int_{y'_1}^{y'_2} E dy'$ , $y' = y/D$ , $y_1 = 0.2D$ , $y_2 = 0.8D$
$f_{bright}$	Factor of brightness of B mode imaging
$f_{cont}$	Factor of contrast of B-mode imaging in response to the color Doppler imaging
$h$	Height of captured images
$H$	Height of PVA-H phantom
$L$	Length of PVA-H phantom
$q$	Flow rate
$r$	Position in the radial direction
$Re$	Reynolds number, $Re = U \cdot D/\nu$
$U$	Mean flow velocity
$\vec{u}$	$\vec{u} = (u, v)$ , flow velocity vector in cylindrical $(z, r)$ coordinate system
$u_{max}$	Maximum velocity in the flow direction
$V$	Measured Doppler velocity (positive value corresponds to the direction toward the probe)
$V_{ana}$	Analytic solution for the Doppler velocity
$V_{max}$	Maximum value of the measured Doppler velocity
$V_{mean}$	Analytic Doppler velocity averaged over the cross section
$V_o$	Maximum Doppler velocity
$w$	Width of captured images
$W$	Width of PVA-H phantom
$y$	Position in the diametral direction
$z$	Position in the flow direction

### Greek letters

$\varphi$	Angle of ultrasonic beam emission
$\theta$	Angle between ultrasonic beam and flow direction

## 2. Materials and Methods

### 2-1 Experimental system

Figure 2 (a) shows an overview of the experimental system. Working fluid, namely, artificial blood (ATS Laboratories, model 707) consisting of water, glycerin, and tracking particles was driven by a constant head tank. The entry region of a straight PVC tube with a length of 2000 mm, a diameter of 10 mm, and a thickness of 1.5 mm, was positioned to ensure a fully developed laminar flow in the PVA-H phantom, a block ( $L \times W \times H = 500 \text{ mm} \times 70 \text{ mm} \times 50 \text{ mm}$ ) with a straight circular tunnel having a diameter of 10 mm. Connectors were placed at the both ends of the tunnel. Details of the PVA-H phantom are explained in the next section. We used a commercial medical ultrasonic diagnostic device (TOSHIBA, SSA-700A). A linear scanning probe (TOSHIBA, PLT-704AT 7.5 MHz) employed for ultrasonic measurement was applied at a position 400 mm from the entrance of the phantom. Figure 2 (b) shows the definition of the angles, namely, the entry angle of the ultrasonic beam,  $\varphi$ , and the angle between the ultrasonic beam and the flow velocity,  $\theta$ . The beam entry angle  $\varphi$  was set at  $70^\circ$  and  $110^\circ$  corresponding to the angle between the ultrasonic beam and the flow velocity  $\theta$  of  $-70^\circ$  and  $-110^\circ$ , respectively. The flow rate was measured by a flowmeter (ATS Laboratories, model 752) and controlled by a flow control valve downstream of the circuit. Figure 3 shows the PVA-H phantom and the ultrasonic probe. The experimental conditions are shown in Table 1.

### 2-2 PVA-H phantom

Poly (vinyl alcohol), PVA, is widely used as an industrial compound, a biomedical medium, and material for food packaging. PVA and the water solution can be easily levigated, and phantoms made of PVA hydrogel (PVA-H) have been used in some previous studies<sup>[26-28]</sup>. PVA-H is a tissue-mimicking material. Compared with conventional phantoms made of silicone rubber or acrylic plastic, PVA-H phantoms are characterized by elasticity and low skin friction due to their high moisture content<sup>[26]</sup>. This high moisture content also means that PVA-H phantoms have an acoustic impedance near that of the living body, and thus enabling ultrasonic measurement<sup>[27, 28]</sup>. The elasticity of the PVA-H can be adjusted in a wide range with PVA of appropriate weight in the water solution; for example, 5% PVA-H has almost the same Young's modulus as the liver<sup>[26]</sup>.

Commercial PVA powder (JAPAN VAM & POVAL, JF-17) was used to make the phantom employed in this study. We made 10 wt% PVA liquid with 300 g of PVA powder and 2700 g of solvent, which was a mixture of 20 wt% water and 80 wt% DMSO (Dimethylsulfoxide). PVA powder was dissolved in the solvent at  $120^\circ\text{C}$  for 120 minutes. After the dissolution, PVA liquid was cast in a stainless box ( $L \times W \times H = 500 \text{ mm} \times 70 \text{ mm} \times 50 \text{ mm}$ ) through which an aluminum cylindrical bar ( $D = 10 \text{ mm}$ ) and two connectors were set.

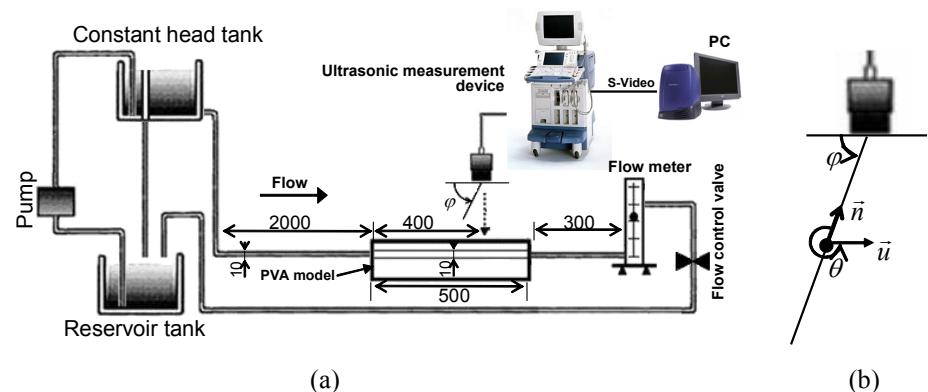


Fig. 2 (a) Overview of experimental system and (b) definition of angles



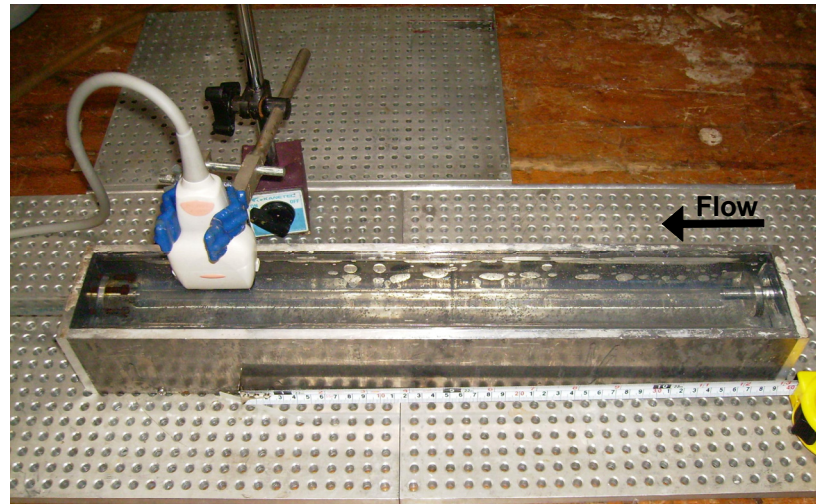


Fig. 3 PVA-H phantom and ultrasonic probe at the measurement position

Table1 Experiment conditions

Angle of ultrasonic beam emission, $\varphi$	$70^\circ$ , $110^\circ$
Angle between ultrasonic beam and flow velocity, $\theta (-180^\circ \leq \theta \leq 180^\circ)$	$-70^\circ$ , $-110^\circ$
Center frequency	7.5 MHz
Pulse repetition frequency	8.5 kHz
Measurement range, $V_o$	9.0 cm/s
Brightness of B-mode imaging, $f_{bright}$	60, 80 (default)
Contrast of color Doppler imaging and B-mode imaging, $f_{cont}$	14 (default), 15
Density of working fluid	$1040 \text{ kg/m}^3$
Kinematic viscosity of working fluid	$1.66 \times 10^{-6} \text{ m}^2/\text{s}$
Picture capture rate	16 Hz
Pixel size	0.05208 mm/pixel

After cooling the PVA solvent to room temperature, the solvent in the box was placed in a freezer at  $-30^\circ\text{C}$  for 24 hours for gelation. We obtained a PVA-H straight tube fluid flow phantom by pulling out the aluminum bar after the gelation.

### 2-3 Method to investigate the C-V relationship

The experiment was performed at a flow rate ranging from  $1.57 \times 10^{-6} \text{ m}^3/\text{s}$  to  $1.16 \times 10^{-5} \text{ m}^3/\text{s}$ , corresponding to  $\text{Re} = 75 - 886$ . As shown by Fig. 2 (a), the site of measurement was  $40 D$  from the inflow of the phantom and there was an additional  $200 D$  straight PVC tube in the upstream region. Therefore, the flow at the measurement position with the maximum Reynolds number  $\text{Re} = 886$ , corresponding to the flow rate  $q = 1.16 \times 10^{-5} \text{ m}^3/\text{s}$  and the mean velocity  $u = 0.148 \text{ m/s}$ , was a fully developed laminar flow since the entrance length was theoretically estimated as  $0.065 \text{ Re} \cdot D = 58D$ .

The color Doppler images ( $w \times h = 720 \text{ pixels} \times 486 \text{ pixels}$ ) of the ultrasonic measurement were transferred to a graphic workstation (SGI, O2) by an s-video cable. We captured 100 contiguous images with a capture frequency of 16 Hz. The maximum Doppler velocity of the measurement range ( $V_o$ ) of the ultrasonic instrument device was held at 9.0 cm/s. The measured Doppler velocity ( $V$ ) ranged between 0.0 and 9.0 cm/s with  $\theta = -70^\circ (\varphi = 70^\circ)$ , and  $-9.0$  and 0.0 cm/s with  $\theta = -110^\circ (\varphi = 110^\circ)$ . Color Doppler images were stored in SGI rgb format or IRIX rgb, which is the standard bitmap format used in the IRIX operation system.

The set of 100 images was transferred and processed in the server (SGI, Prism). The intensities of red, green, and blue at each pixel on the images were extracted by an original program. We obtained the temporal average of 100 images in the whole domain first, and then the spatial average in the flow direction (350 pixels). In previous studies<sup>[14]</sup>, the relationship between the color Doppler value and the Doppler velocity (C-V relationship) was obtained by analyzing the color bar in the captured images (Fig. 4 (a)). Figure 4 (b) shows the C-V relationship obtained with the method employed in the previous study. The sign of the Doppler velocity was determined by comparing the color Doppler values of red and blue. The amplitude of the Doppler velocity was almost proportional to the color Doppler value of green.

In the present study, we obtained the C-V relationship by comparing the maximum value of green in each distribution of the color Doppler value with the corresponding velocity of the analytic solution.

## 2-4 Visual adjustment factor of ultrasonic instrument

Several visual adjustment factors are possible with the present ultrasonic instrument. Among them, two factors may influence the Doppler velocity measurement: the factor  $f_{bright}$  of the brightness of the B-mode imaging and the factor  $f_{cont}$  of the contrast of the B-mode imaging with respect to the color Doppler imaging. Since the effect of these factors on the velocity measurement was not clear, it was also investigated in this study.

The brightness factor  $f_{bright}$  may change from 60 to 100 in the present system. The B-mode image of the object is invisible on the monitor at  $f_{bright} = 60$ , and the intensity increases as the factor increases. The contrast factor  $f_{cont}$  may change from 0 to 15. Only the B-mode image is displayed for  $f_{cont} = 0$ , and the intensity of the color Doppler image increases as the factor increases. Figures 5 (a) and (b) show examples of the captured image at  $Re = 690$  with  $\theta = -70^\circ$  and  $f_{cont} = 14$  (default) with two different  $f_{bright}$  values. The default setting of the factor  $f_{bright} = 80$  and  $f_{cont} = 14$  are used hereafter.

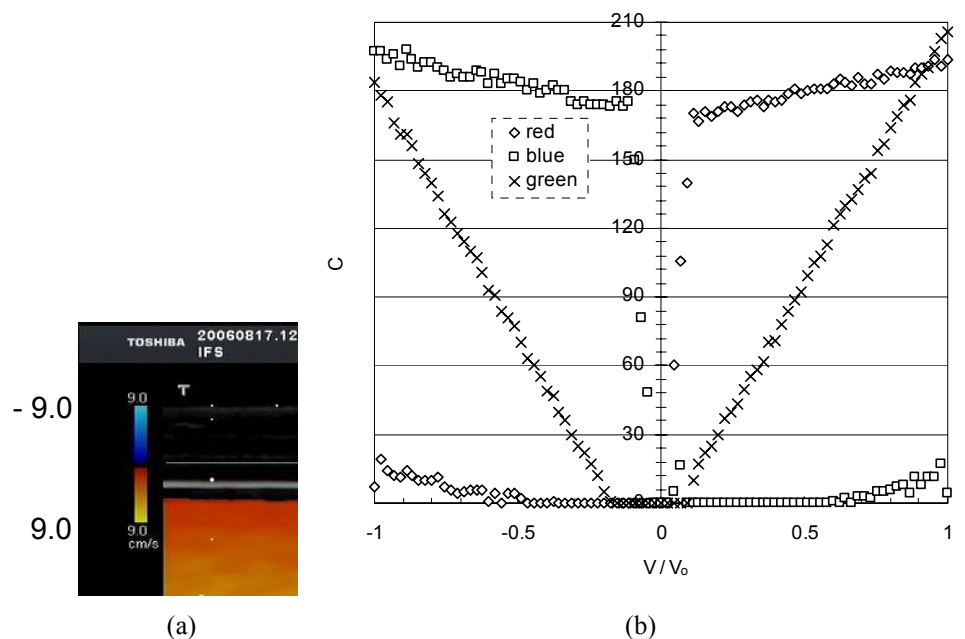


Fig. 4 (a) Color bar and (b) C-V relationship shown by the color bar

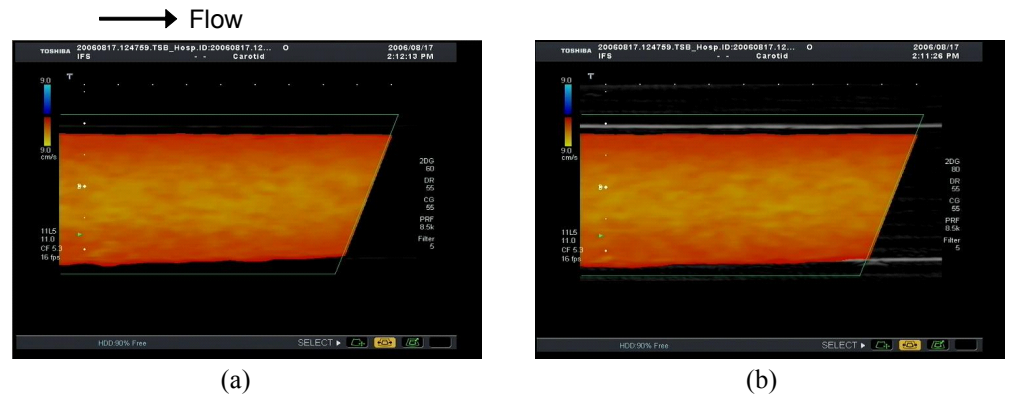


Fig. 5 Color Doppler image for  $q = 8.83 \times 10^{-6} \text{ m}^3/\text{s}$ ,  $Re = 690$ ,  $\theta = -70^\circ$ ,  $f_{cont} = 14$  with (a)  $f_{bright} = 60$  and (b)  $f_{bright} = 80$  (default)

### 3. Results and Discussion

#### 3-1 C-V relationship

The color Doppler image was obtained for the range of Reynolds number between  $Re = 75$  and  $860$  for  $\theta = -70^\circ$ , and between  $Re = 102$  and  $886$  for  $\theta = -110^\circ$ . Aliasing was observed for Reynolds numbers larger than the range for each beam  $\theta$ . It should be noted that the maximum Reynolds number depends on the beam angle and is larger than that for the specified measurement range for  $V_{max} = V_o$  ( $Re = 794$  and  $q = 1.03 \times 10^{-5} \text{ m}^3/\text{s}$ ).

Figures 6 (a) and (b) show the distribution of the color Doppler value in the diametral direction at each flow rate for  $\theta = -70^\circ$  and  $\theta = -110^\circ$ , respectively. It should be noted that each result was obtained from 100 sequential images by averaging in time and then averaging in space in the axial direction. The distributions of the color Doppler value are not parabolic, which implies that the former linear C-V relationships are not valid.

By comparing the maximum color Doppler value with the maximum velocity of the analytic solution at the center for each case, we obtained the C-V relationship shown by the symbols  $\circ$  and  $\times$  in Fig. 7 for the B-mode contrast factors  $f_{cont} = 14$  (default) and  $15$ , respectively. C-V relationships for  $\theta = -70^\circ$  and  $\theta = -110^\circ$  are different but are both nonlinear. There is little difference between the results with  $f_{cont} = 14$  and  $15$ , so we deal with the case of  $f_{cont} = 14$  (default) in the following.

We obtained the polynomial function to approximate each C-V relationship as

$$\begin{aligned} \frac{V}{V_o} = & -3.32 \times 10^{-12} \cdot C^6 + 1.65 \times 10^{-9} \cdot C^5 - 3.09 \times 10^{-7} \cdot C^4 + 2.65 \times 10^{-5} \cdot C^3 \\ & - 9.75 \times 10^{-4} \cdot C^2 + 1.74 \times 10^{-2} \cdot C \quad \text{for } \theta = -70^\circ \end{aligned} \quad (1)$$

$$\begin{aligned} \frac{V}{V_o} = & -4.57 \times 10^{-9} \cdot C^4 + 1.50 \times 10^{-6} \cdot C^3 - 1.49 \times 10^{-4} \cdot C^2 - 3.82 \times 10^{-3} \cdot C \\ & \text{for } \theta = -110^\circ \end{aligned}$$

The solid lines in Fig. 7 based on Eq. (1) agree well with the measurement data. The broken lines in Fig. 7 are based on the approximate functions obtained from the green data of the color bar in Fig. 4 (b) as

$$\begin{aligned} \frac{V}{V_o} = & 4.51 \times 10^{-3} \cdot C + 0.067 \quad \text{for } \theta = -70^\circ \\ \frac{V}{V_o} = & -4.53 \times 10^{-3} \cdot C - 0.17 \quad \text{for } \theta = -110^\circ \end{aligned} \quad (2)$$

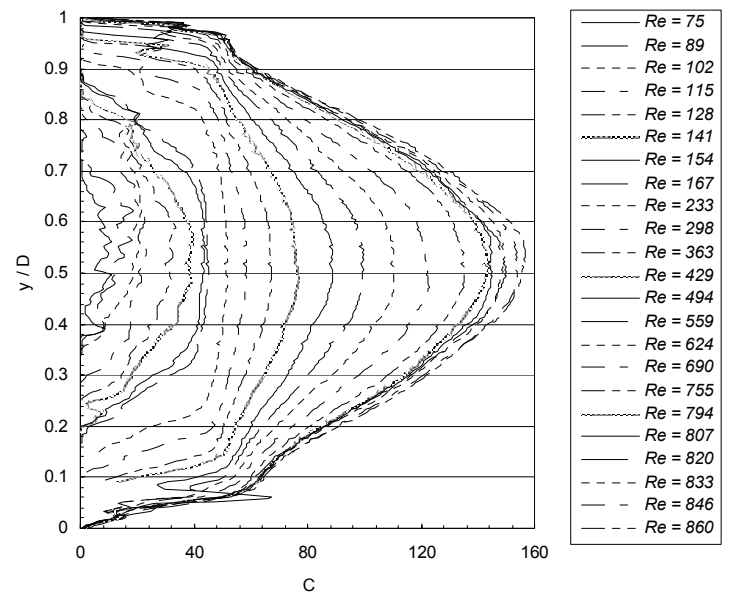
The present C-V relationships (Eq. (1)) are different from the ones obtained from the color bar (Eq. (2)).

We converted measured color Doppler values to Doppler velocities with both of the C-V relation functions. Figure 8 shows an example for the converted Doppler velocity

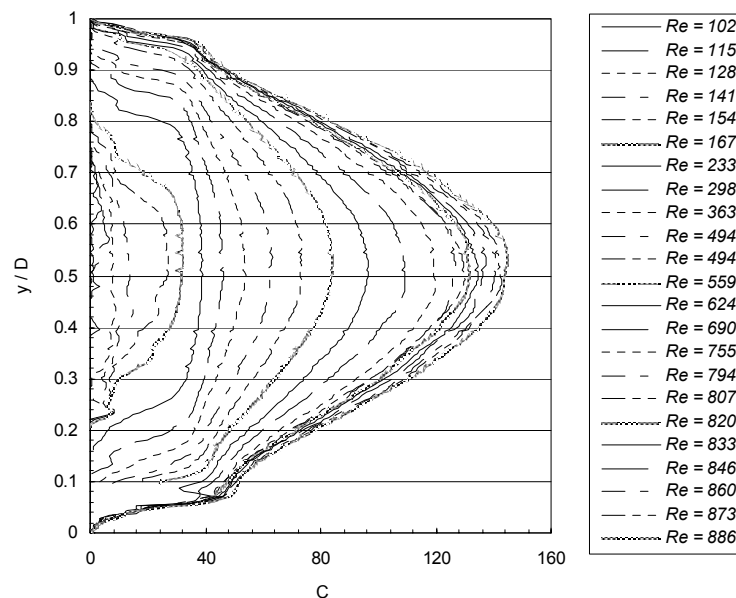


distributions for  $\theta = -70^\circ$  and  $\theta = -110^\circ$  at  $Re = 690$  compared with the analytic solutions. The velocity distributions based on the present C-V relationships agree with the analytic solutions except in the region near the wall, while those with the former C-V relationships do not agree in the whole region.

The influence of  $f_{bright}$  on the Doppler velocity measurement is shown in Fig. 8 for  $\theta = -70^\circ$ . The result of  $f_{bright} = 60$  is essentially the same as that of  $f_{bright} = 80$  (default) showing good agreement with the analytical solution except in the region near the tube walls. Doppler velocity measurement with  $f_{bright} = 60$ , which is free from the influence of B-mode imaging, does not improve the accuracy of velocity measurement near the wall.



(a)



(b)

Fig. 6 Distribution of the color Doppler value in the diametral direction with  $f_{cont} = 14$ ,  $f_{bright} = 80$  for (a)  $\theta = -70^\circ$  and (b)  $\theta = -110^\circ$



These results suggest the possibility that the measurement data near the wall should be removed from the feedback signal of UMI simulation. In addition, the technique to extract the vessel boundary from the color Doppler image is an important problem, but is beyond the scope of the present paper.

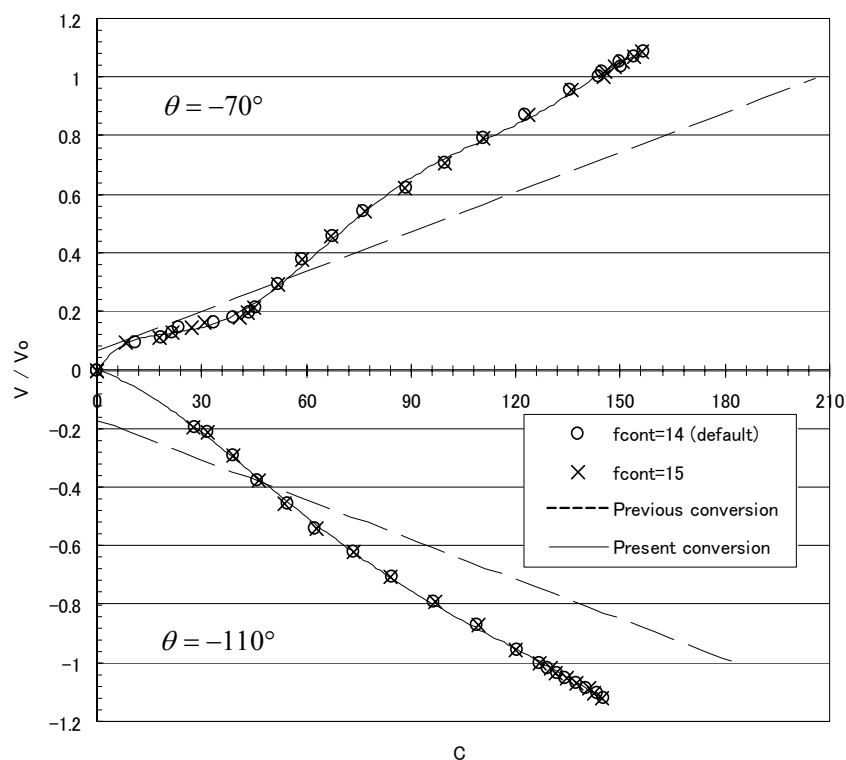


Fig. 7 Comparison of C-V relationships and conversion functions

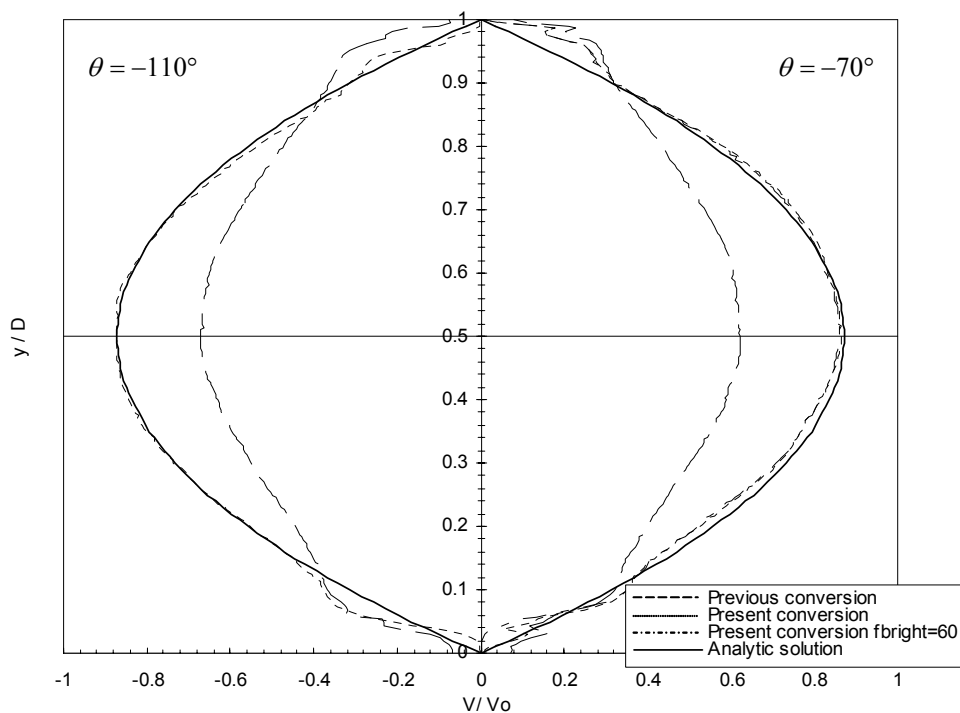


Fig. 8 Comparison of converted Doppler velocities (  $Re = 690$  )

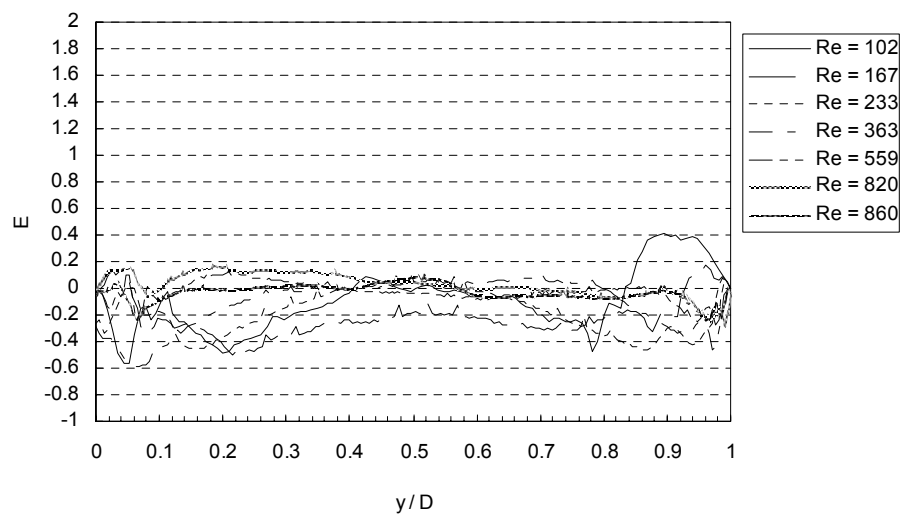
### 3-2 Accuracy of ultrasonic measurement

Figures 9 (a) and (b) show the normalized error  $E$  in Doppler velocity along the diameter for various Reynolds numbers with the beam angles  $\theta = -70^\circ$  and  $\theta = -110^\circ$ , respectively. The normalized error is defined as

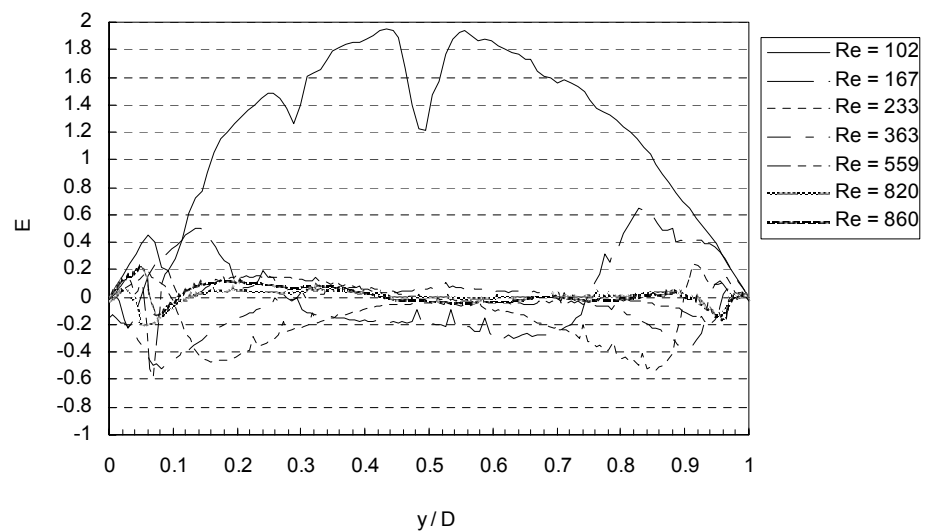
$$E = \frac{V - V_{ana}}{V_{mean}}, \quad (3)$$

where  $V_{ana}$  is the analytic solution for the Doppler velocity and  $V_{mean}$  is the average value of  $V_{ana}$ . The error is relatively large in the case of low Reynolds number, as well as in the region near the wall.

Figure 10 shows the distribution of the normalized error  $E$  with the Reynolds number for representative points along the diametral direction. The figure shows that the relative error is larger for small Doppler velocities. It is noted that the relative error near the tube wall (broken lines) is larger than that near the tube axis (solid lines) in the region of small Doppler velocities.



(a)



(b)

Fig. 9 Normalized error in Doppler velocity in the diametral direction for various Re with  
(a)  $\theta = -70^\circ$  and (b)  $\theta = -110^\circ$

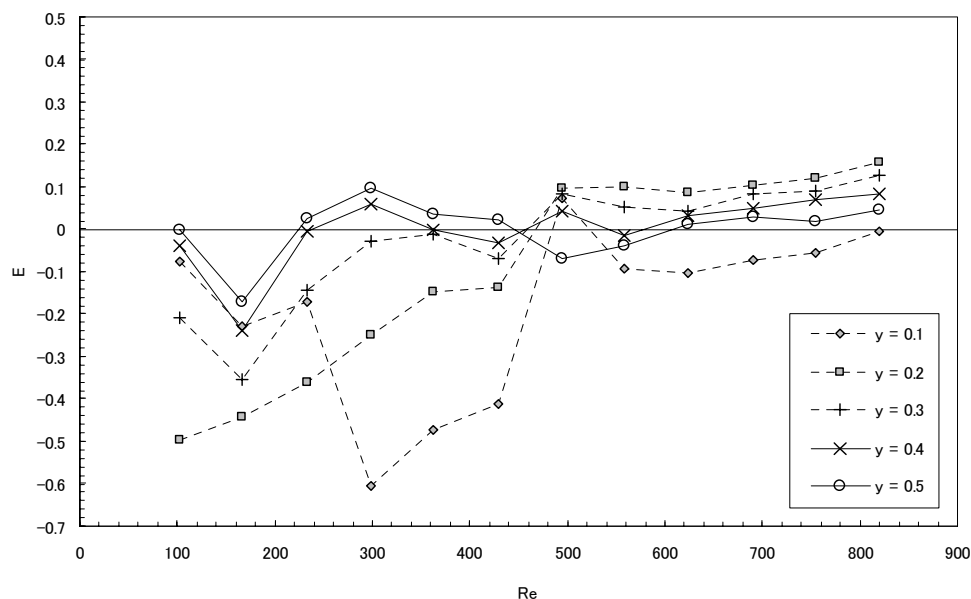


Fig. 10 Normalized error with Reynolds number at representative points in the diametral direction ( $\theta = -70^\circ$ )

Based on the above results, Fig. 11 shows the normalized error  $E_{ave}$  averaged in the region near the center of the tube between  $0.2 D$  and  $0.8 D$  in the diametral direction. With increasing Reynolds number, the relative error first decreases and then remains almost constant below 10% for the Reynolds numbers larger than 500.

From the above examination, we confirmed that the measurement results converted with the proposed C-V relationships are reliable for high Reynolds number cases but that the results near the wall contain much measurement error compared with those near the center of the tube. In order to perform the UMI simulation precisely, the experimental data fed back to the numerical simulation should be as precise as possible. Thus, these results suggest that the precise part of the measurement data obtained with an appropriate setting for the range  $V_o$  of Doppler velocity measurement be used for feedback.

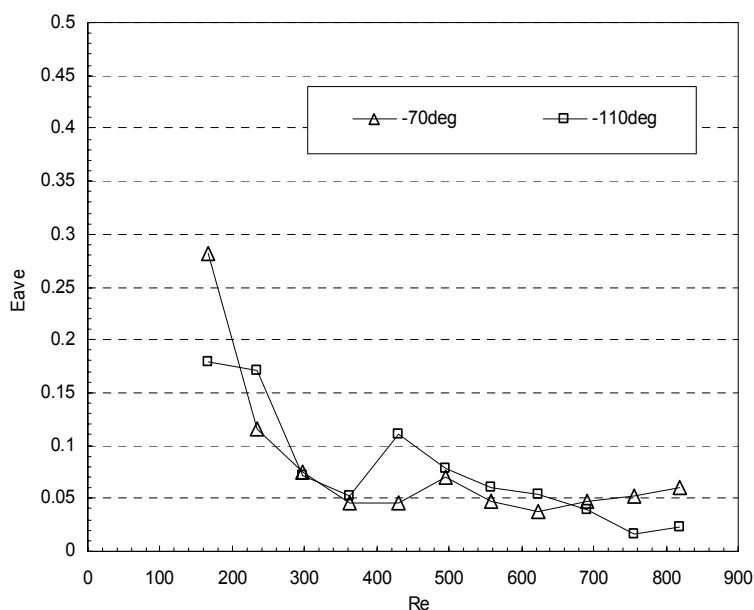


Fig. 11 Averaged normalized error with Reynolds number

### 3-3 Temporal and spatial averaging of ultrasonic measurement data

As noted in the above-mentioned examination, the ultrasonic measurement data averaged both temporally and spatially reproduce the velocity distribution of a steady laminar flow correctly except in the region near the tube wall. However, actual blood flow changes in time and space. Therefore, the number of data to take an average is limited to ensure appropriate spatial and temporal resolutions. On the other hand, reducing the number of data for averaging increases the effect of measurement noise. In this section, we examine the effect of temporal and spatial averaging of the ultrasonic measurement.

Figure 12 shows the distribution of the Doppler velocity for  $Re = 690$  and  $\theta = -70^\circ$  at one cross section temporally averaged using different numbers of sequential data ranging from 1 to 100 images. Increasing the number of averaging data results in closer agreement with the analytic solution.

Figure 13 shows the result at one point of time spatially averaged using different numbers of neighboring data ranging from 1 to 300 pixels. Similar to the former case, increasing the number of spatial averagings results in better agreement with the analytic solution.

Finally, we investigated the decrease of error in relation to the number of temporal and spatial averagings. We evaluated the decrease of the error  $E_{ave}$  in relation to the increase in the number of temporal averaging data for 6 cross-sections 2.604 mm apart and in relation to the number of spatial averaging data for 6 points of time at intervals of 1.25 s. Figure 14 shows that the error monotonically decreases with an increase in the number of averaging data. For example, an error of 5% was achieved by temporal averaging with 20 data at time intervals of 1.25 s or by spatial averaging of 50 data for an axial length of 2.604 mm. A combination of temporal and spatial averaging would possibly further reduce the error. The above results are essential for evaluation of the accuracy and resolution of the UMI simulation of real blood flow.

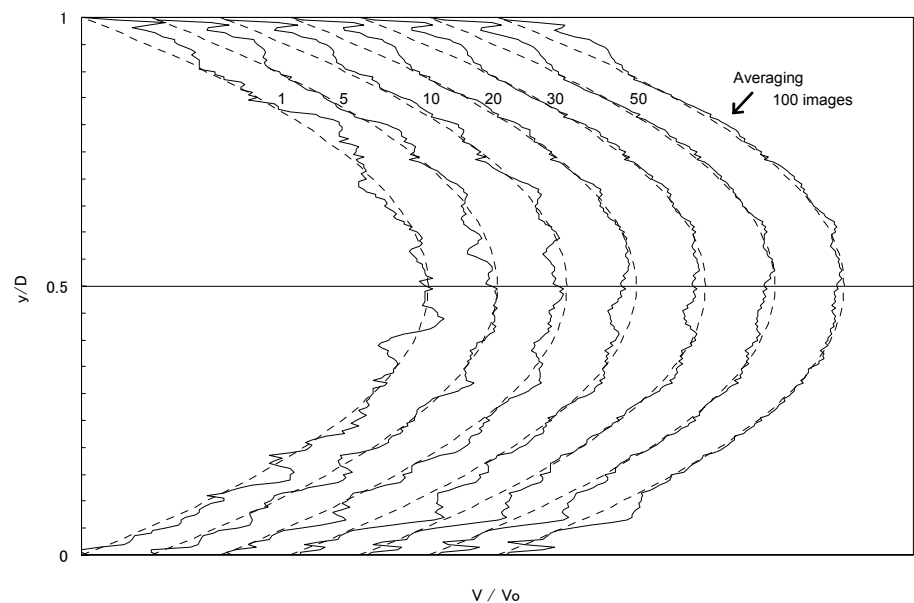


Fig. 12 Effect of temporal averaging at one cross section ( $Re = 690$ ,  $\theta = -70^\circ$ )  
Broken lines and solid lines show the analytic solution of  $V / V_o$  and its converted results, respectively.



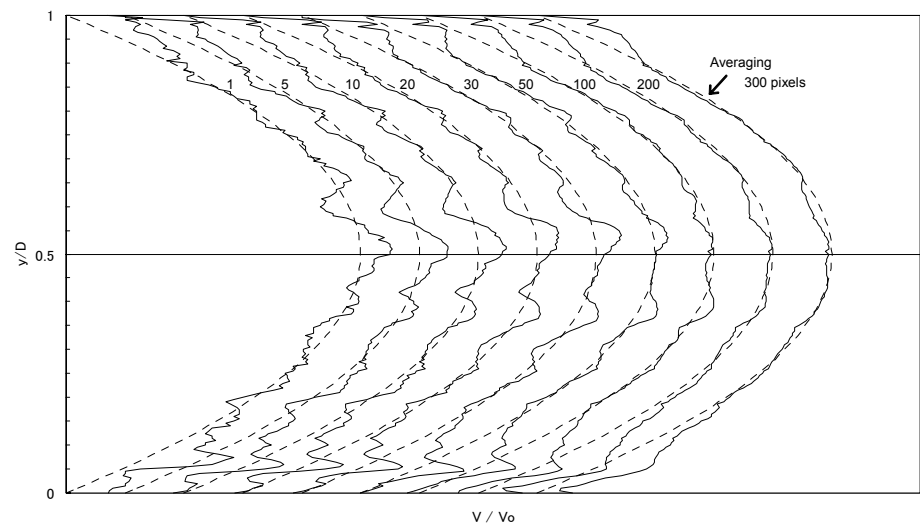


Fig. 13 Effect of spatial averaging at one point of time ( $Re = 690, \theta = -70^\circ$ )

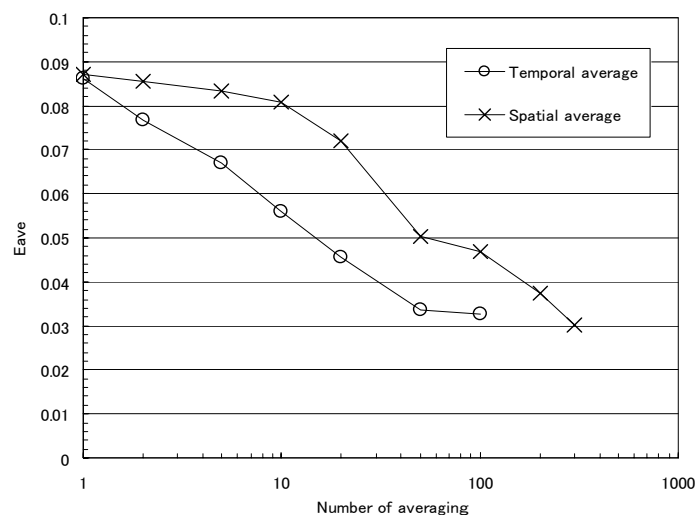


Fig. 14 Averaged normalized error with the number of temporal or spatial averagings ( $Re = 690, \theta = -70^\circ$ )

#### 4. Summary

In this study, we performed ultrasonic measurement with a PVA-H fluid flow phantom as a fundamental study for experimental validation of Ultrasonic-Measurement-Integrated (UMI) simulation.

We developed an experimental system utilizing a PVA-H phantom. By measuring a developed laminar flow through a straight circular tunnel inside the phantom and analyzing the measured color Doppler images, we obtained a relationship between the color Doppler value and the Doppler velocity. This C-V relationship was confirmed at two angles between the ultrasonic beam and the flow velocity,  $\theta = -70^\circ$  and  $\theta = -110^\circ$ . The velocity distribution converted from the present C-V relationships showed far better agreement with the analytic solution than that converted from the C-V relationships obtained by the color bar. The investigation of the normalized error  $E$  confirmed that the result obtained with the present C-V relationships was reliable for relatively high Reynolds numbers, but that the accuracy near the wall was somewhat degraded.

Investigation of the influences of two signal conditioning factors, namely, the brightness of B-mode imaging and the contrast of color Doppler imaging and B-mode imaging showed that these factors had little effect on the velocity measurement results.

Furthermore, we investigated the effect of temporal and spatial averaging of ultrasonic measurement data as a fundamental consideration of the UMI simulation of real blood flow. In both temporal and spatial averaging, increasing the number of averaging data resulted in a better agreement with the analytic solution.

The results obtained in this paper confirmed that a commercial medical ultrasonic device is applicable in a flow domain except near the wall by properly evaluating the C-V relationship. It was suggested that setting an appropriate measurement range for the blood flow condition and appropriate temporal averaging of the measurement data would result in UMI simulation with high accuracy. Based on these results, experimental validation and a trial application of real UMI simulation will be conducted in the future.

### Acknowledgement

The authors acknowledge the support received from the Future Medical Engineering Based on Bio-nanotechnology Program (21 COE Program) and the Global COE Program "Global Nano-Biomedical Engineering Education and Research Network Centre." The signal processing was performed on the Integrated Supercomputing System in the Advanced Fluid Information Research Center, Institute of Fluid Science, Tohoku University.

### References

- [1] Fry DL: Acute Vascular Endothelial Changes Associated with Increased Blood Velocity Gradients. *Circulation Research*, Vol. 22, No.2, (1968), pp. 165-197.
- [2] Reidy MA, Bowyer DE: Scanning Electron Microscopy of Arteries. The Morphology of Aortic Endothelium in Haemodynamically Stressed Areas Associated with Branches. *Atherosclerosis*, Vol. 26, No. 2, (1977), pp. 181-194.
- [3] Caro CG: Mechanical Factors in Atherogenesis. In: Hwang NHC, Norman NA, eds. Cardiovascular flow dynamics and measurements. *Baltimore: University Park Press*, (1997), pp. 473-487.
- [4] Zarins CK, Giddens DP, Bharadvaj BK, Sottiurai VS, Mabon RG, Glagov S: Carotid Bifurcation Atherosclerosis. Quantitative Correlation of Plaque Localization with Flow Velocity Profiles and Wall Shear Stress. *Circulation Research*, Vol. 53 (1983), pp. 502-514.
- [5] Ku DN, Giddens DP, Zarins CK, Glagov S: Pulsatile Flow and Atherosclerosis in the Human Carotid Bifurcation. Positive Correlation Between Plaque Location and Low Oscillating Shear Stress. *Arteriosclerosis*, Vol. 5, (1985), pp. 293-302.
- [6] Krueger JW, Young DF, Cholvin NR: An in vitro Study of Flow Response by Cells. *Journal of Biomechanics*, Vol. 4, (1971), pp. 31-36.
- [7] Remuzzi A, Dewey CF, Davis PF, Gimbrone MA, Jr: Orientation of Endothelial Cells in Shear Fields in vitro. *Biorheology*, Vol. 21, (1984), pp. 617-630.
- [8] Flora HS, Talei-Faz B, Ansdell L, Chaloner JE, Sweeny A, Grass A, Adiseshiah E: Aneurysm Wall Stress and Tendency to Rupture Are Features of Physical Wall Properties: an Experimental Study. *Journal of Endovascular Therapy*, Vol. 9, (2002), pp. 665-675.
- [9] Papathanasopoulou P, Zhao S, Köhler U, Robertson MB, Long Q, Hoskins P, Xu XY, Marshall I: MRI Measurement of Time-resolved Wall Shear Stress Vectors in a Carotid Bifurcation Model, and Comparison with CFD Predictions. *Journal of Magnetic Resonance Imaging*, Vol. 17, No. 2, (2003), pp. 153-162.
- [10] Marshall I, Zhao S, Papathanasopoulou P, Hoskins P, Xu XY: MRI and CFD Studies of Pulsatile Flow in Healthy and Stenosed Carotid Bifurcation Models. *Journal of*

- Biomechanics*, Vol. 37, No. 5, (2004), pp. 679-687.
- [11] Steinman. DA: Image-based Computational Fluid Dynamics Modeling in Realistic Arterial Geometries. *Annals of Biomedical Engineering*, Vol. 30, No. 4 (2002), pp. 483-497.
- [12] Liu Y, Lai Y, Nagaraj A, Kane B, Hamilton A, Greene R, McPherson DD, Chandran KB: Pulsatile Flow Simulation in Arterial Vascular Segments with Intravascular Ultrasound Images. *Medical Engineering and Physics*, Vol. 23, No. 8, (2001), pp. 583-595.
- [13] Di Martino ES, Guadagni G, Fumero A, Ballerini G, Spirito R, Biglioli P, Redaelli A: Fluid-Structure Interaction within Realistic Three-Dimensional Models of the Aneurysmatic Aorta as a Guidance to Assess the Risk of Rupture of the Aneurysm. *Medical Engineering and Physics*, Vol. 23, No. 9, (2001), pp. 647-655.
- [14] Funamoto K, Hayase T, Shirai A, Saijo Y, Tambe T: Fundamental Study of Ultrasonic-Measurement-Integrated Simulation of Real Blood Flow in the Aorta. *Annals of Biomedical Engineering*, Vol. 33, No. 4, (2005), pp. 415-428.
- [15] Hayase T, Hayashi S: State Estimator of Flow as an Integrated Computational Method with the Feedback of Online Experimental Measurement. *Journal of Fluids Engineering-Transactions of the ASME*, Vol. 119, No. 4, (1997), pp. 814-822.
- [16] Funamoto K, Hayase T, Saijo Y, Tambe T: Detection and Correction of Aliasing in Ultrasonic Measurement of Blood Flows with Ultrasonic-Measurement-Integrated Simulation. *Technology and Health Care*, Vol. 13, (2005), pp. 331-345.
- [17] Funamoto K, Hayase T, Saijo Y, Tambe T: Effect of Ultrasound Probe Placement in Ultrasonic-Measurement-Integrated Simulation of Blood Flows. *Proceedings of the ICBME*, (2005), CD-ROM.
- [18] Funamoto K, Hayase T, Saijo Y, Tambe T: Numerical Study on Variation of Feedback Methods in Ultrasonic-Measurement-Integrated Simulation of Blood Flow in the Aneurysmal Aorta. *JSME International Journal Series C*, Vol. 49, (2006), 144-155.
- [19] Biomedical Engineering Handbook, Second Edition, Ed. Bronzino, J.D., 1 (2000), CRC Press.
- [20] Chihara K: Ultrasound (in Japanese), (2001), Corona Pub. Corp.
- [21] Boote EJ, Zagzebski JA: Performance Tests of Doppler Ultrasound Equipment with a Tissue and Blood-mimicking Phantom. *Ultrasound in Medicine and Biology*, Vol. 8, (1988), pp. 73-85.
- [22] Fleming AD, McDicken WN, Sutherland GR, Houkins PR: Assessment of Colour Doppler Tissue Imaging Using Test-phantoms. *Ultrasound in Medicine and Biology*, Vol. 20, (1994), pp. 937-951.
- [23] Rickey DW, Rankin R, Fenster A: A Velocity Evaluation Phantom for Colour and Pulsed Doppler Instruments. *Ultrasound in Medicine and Biology*, Vol. 18, (1992), pp. 479-494.
- [24] Tysoe C, Evans DH: Bias in Mean Frequency Estimation of Doppler Signals Due to Wall Clutter Filters. *Ultrasound in Medicine and Biology*, Vol. 21, (1995), pp. 671-677.
- [25] Willemetz JC, Nowicki A, Meister JJ: Bias and Variance in the Estimate of the Doppler Frequency Induced by a Wall Motion Filter. *Ultrasonic Imaging*, Vol. 11, (1989), pp. 215-225.
- [26] Ohta M, Handa A, Iwata H, Rufenecht DA, Tsutsumi S: Poly-vinyl Alcohol Hydrogel Vascular Models for in vitro Aneurysm Simulations: The Key to Low Friction Surfaces. *Technology and Health Care*, Vol. 12, (2004), pp. 225-233.
- [27] Seemantini KN, Hillary A, Greg M, Derek B, Aaron F: A Pulsating Coronary Vessel Phantom for Two- and Three-Dimensional Intravascular Ultrasound Studies. *Ultrasound in Medicine and Biology*, Vol. 29, (2003), pp. 621-628.
- [28] Surry KJM, Austin HJB, Fenster A, Peters TM: Poly(vinyl alcohol) Cryogel Phantoms for Use in Ultrasound and MR Imaging. *Physics in Medicine and Biology*, Vol.49, (2004), pp. 5529-5546.